

# White light generation of glass ceramics containing Ba<sub>2</sub>LaF<sub>7</sub>: Eu<sup>2+</sup>, Tb<sup>3+</sup> and Sm<sup>3+</sup> nanocrystals

Yang Xu (徐扬)<sup>1</sup>, Shuo Cui (崔硕)<sup>1</sup>, Hengyi Fu (傅恒毅)<sup>1</sup>, Jiangyun Qian (钱江云)<sup>1</sup>, Qun Luo (骆群)<sup>1</sup>, Xusheng Qiao (乔旭升)<sup>1\*</sup>, Xianping Fan (樊先平)<sup>1</sup>, and Xianghua Zhang (章向华)<sup>2</sup>

<sup>1</sup>Department of Materials Science and Engineering, Zhejiang University, Hangzhou 310027, China

<sup>2</sup>UMR-CNRS 6512 "Verres and Ceramiques", Institut de Chimie de Rennes, Universite de Rennes 1-Campus de Beaulieu, 35042 Rennes Cedex-France

\*Corresponding author: qiaoxus@zju.edu.cn

Received August 15, 2011; accepted September 15, 2011; posted online November 18, 2011

The Eu<sup>2+</sup>/Tb<sup>3+</sup>/Sm<sup>3+</sup> co-doped oxyfluoride glass ceramics containing Ba<sub>2</sub>LaF<sub>7</sub> nanocrystals are prepared in the reducing atmosphere. The X-ray diffraction results show that Eu<sup>2+</sup>, Tb<sup>3+</sup> and Sm<sup>3+</sup> ions are enriched into the precipitated Ba<sub>2</sub>LaF<sub>7</sub> nanophase after the annealing process. It deduces efficient energy transfers from Eu<sup>2+</sup> to Tb<sup>3+</sup> and Sm<sup>3+</sup> and intensifies warm white luminescence of the glass ceramics. Comparing with the glass, the luminescence quantum yield of the glass ceramics is also enlarged by about 3 times. This demonstrates the potential white light-emitting diode application of the glass ceramics produced in this letter.

OCIS codes: 160.2540, 160.5690, 160.6990.

doi: 10.3788/COL201210.031602.

White light-emitting diodes (LEDs) are considered new generation illumination technology, since they have longer lifetimes, highly efficiency, better reliability, and are environment-friendly<sup>[1–3]</sup>. The development of very efficient ultraviolet (UV)/blue LEDs based on a wide-band gap semiconductor, such as GaN, has led to considerable progress in the field of solid-state lighting as well as backlighting for display application<sup>[4,5]</sup>. Although white light is easily achieved in a YAG:Ce-based system, the individual degradation rate between the blue LED and yellow phosphor causes chromatic aberration and poor white light performance after long working periods<sup>[6]</sup>. Glass ceramics might be good alternatives for white LEDs (WLEDs), due the following advantages: heat resistance, easy formability, and low porosity compared with sintered ceramics<sup>[7–12]</sup>. The oxyfluoride glass ceramics are considered ideal rare earth ion hosts, because such materials combine the excellent luminescent environment of fluoride crystals and good chemical stability of oxide glass<sup>[13,14]</sup>. In this letter, Eu<sup>2+</sup>/Tb<sup>3+</sup>/Sm<sup>3+</sup> co-doped fluorosilicate glass ceramics containing Ba<sub>2</sub>LaF<sub>7</sub> nanocrystals are investigated as WLED materials. The Eu<sup>2+</sup> ions are characterized by their broad and intense f-d absorption and emission bands in ultraviolet to visible range that are widely utilized as phosphor dopants<sup>[15,16]</sup>. The efficient energy transfers (ETs) from Eu<sup>2+</sup> to Tb<sup>3+</sup> and Sm<sup>3+</sup> bring strong luminescence of materials, and red emission from Sm<sup>3+</sup> is ideal in improving the color rendering index (CRI).

Oxyfluoride glass with the composition of 45SiO<sub>2</sub>-15Al<sub>2</sub>O<sub>3</sub>-7La<sub>2</sub>O<sub>3</sub>-12Na<sub>2</sub>O-15BaF<sub>2</sub>-0.3EuF<sub>2</sub>-2.7TbF<sub>3</sub>-3SmF<sub>3</sub> was prepared by melting appropriate batch materials (SiO<sub>2</sub>, Al<sub>2</sub>O<sub>3</sub>, La<sub>2</sub>O<sub>3</sub>, Na<sub>2</sub>CO<sub>3</sub>, BaF<sub>2</sub>, EuF<sub>3</sub>, TbF<sub>3</sub>, and SmF<sub>3</sub>) in covered corundum crucibles at about 1350°C for 35 min. A reducing atmosphere was applied by using carbon crucibles and carbon granules to reduce Eu<sup>3+</sup> to Eu<sup>2+</sup> ions during melting. To obtain the

glass, the melt was poured on a brass mould, which was then pressed by another brass plate. The glass ceramic sample was obtained by annealing the glass for 2 hat 630 °C. The glass and glass ceramics were polished on a UNJ-POL-802 precision lapping/polishing machine.

X-ray diffraction (XRD, XD-98) measurements were performed with Cu-Kα radiation at 4 deg./min scanning rate. Photoluminescence (PL) spectra and decay curves were measured with spectrometer (Edinburgh FLS92P, Edinburgh Instruments Ltd, UK), using excitation of microsecond and nanosecond flash lamps. The scattering and emission spectra were also recorded by a Hamamatsu R928 PMT, which was equipped with an integrating sphere on the FLS920 fluorescence spectrometer. Then, quantum yields (η) were determined using

$$\eta_{\text{QY}} = \frac{\varepsilon}{\alpha} = \frac{\int L_{\text{emission}}}{\int E_{\text{blank}} - \int E_{\text{sample}}}. \quad (1)$$

Quantum yield (η) is the percentage of the photon number emitted by the sample (ε) versus the photon number absorbed by the sample (α). In Eq. (1), L<sub>emission</sub> is the emission spectrum of the sample, E<sub>sample</sub> is the scattering spectrum of the light used to excite the sample, and E<sub>blank</sub> is the scattering spectrum of the light used for excitation without any sample in the sphere. All measurements were performed at room temperature.

The glass transition temperatures (T<sub>g</sub>) and crystallization peak temperatures (T<sub>c</sub>) of the glass samples can be determined from the DTA curves. The glass samples have T<sub>g</sub>, T<sub>c1</sub>, and T<sub>c2</sub> of 595, 660, and 820 °C, respectively. According to the heat treatment of the glass around T<sub>c</sub> and the subsequent XRD analysis, T<sub>c1</sub> corresponds to the precipitation of cubic Ba<sub>2</sub>LaF<sub>7</sub> phase, and T<sub>c2</sub> corresponds to the crystallization process of the whole glass components. Accordingly, we annealed the glass samples at

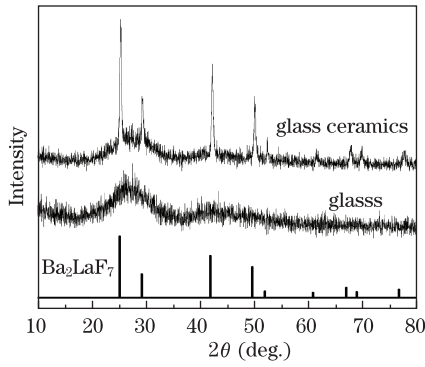


Fig. 1. XRD patterns of the  $45\text{SiO}_2\text{-}15\text{Al}_2\text{O}_3\text{-}7\text{La}_2\text{O}_3\text{-}12\text{Na}_2\text{O-}15\text{BaF}_2\text{-}0.3\text{EuF}_2\text{-}2.7\text{TbF}_3\text{-}3\text{SmF}_3$  glass and glass ceramics.

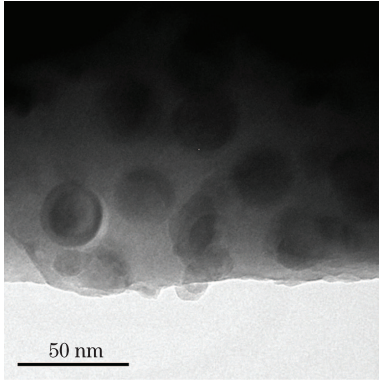


Fig. 2. TEM images of the  $45\text{SiO}_2\text{-}15\text{Al}_2\text{O}_3\text{-}7\text{La}_2\text{O}_3\text{-}12\text{Na}_2\text{O-}15\text{BaF}_2\text{-}0.3\text{EuF}_2\text{-}2.7\text{TbF}_3\text{-}3\text{SmF}_3$  glass ceramics.

630 °C for 2 h to obtain the transparent glass ceramic samples containing cubic  $\text{Ba}_2\text{LaF}_7$  nanophase. XRD patterns of the glass ceramic sample (Fig. 1) show diffraction peaks on the broad glassy diffraction base, which are easily assigned to cubic  $\text{Ba}_2\text{LaF}_7$ . From the XRD data, the crystal size, crystallinity, and lattice parameter of the cubic  $\text{Ba}_2\text{LaF}_7$  are determined as  $25.8 \pm 1.4$  nm,  $26.8 \pm 0.8$  %, and  $6.045$  Å, respectively (see Table 1). Due to size of the precipitated  $\text{Ba}_2\text{LaF}_7$  nanocrystals, which is much smaller than the wavelength of the visible light, the glass ceramics maintain high optical transparency. It indicates that a number of rare earth ions ( $\text{Eu}^{2+}$ ,  $\text{Tb}^{3+}$ , and  $\text{Sm}^{3+}$ ) have enriched in the precipitated  $\text{Ba}_2\text{LaF}_7$  nanocrystals. In order to keep electric charge balance,  $\text{Eu}^{2+}$  ions are used as substitute for the  $\text{Ba}^{2+}$  sites, whereas  $\text{Tb}^{3+}$  and  $\text{Sm}^{3+}$  usually occupy the  $\text{La}^{3+}$  sites. Since the ionic radius of  $\text{Eu}^{2+}$  (0.125 nm) is smaller than  $\text{Ba}^{2+}$  (0.144 nm), and those of  $\text{Tb}^{3+}$  (0.100 nm) and  $\text{Sm}^{3+}$  (0.104 nm) are also smaller than  $\text{La}^{3+}$  (0.113 nm), the lattice parameters of  $\text{Ba}_2\text{LaF}_7$ :  $\text{Eu}^{2+}$ ,  $\text{Tb}^{3+}$ ,  $\text{Sm}^{3+}$  become smaller than the standard. Figure 2 shows the TEM image of the glass ceramics. The gray background and the black circular spots correspond to the glass phase and the precipitated  $\text{Ba}_2\text{LaF}_7$  nanocrystals, respectively. The size of the roughly spherical particles that are distributed homogeneously in the glass matrix are approximately 25–30 nm, which is consistent with the Scherrer-calculated diameter.

Figure 3 shows the excitation PL spectra of the glass and glass ceramics. When monitoring with 454-nm PL, the samples present a broad excitation band from 200

to 450 nm, which can be assigned to the  $4f \rightarrow 5d$  transitions of  $\text{Eu}^{2+}$ . However, when monitoring with the 542-nm PL of  $\text{Tb}^{3+}$ :  ${}^5\text{D}_4 \rightarrow {}^7\text{F}_5$ , we cannot recognize the f-f transition peaks from the excitation spectra; instead, we observe a similar excitation band with that of  $\text{Eu}^{2+}$ . Thus, there are ETs from  $\text{Eu}^{2+}$  to  $\text{Tb}^{3+}$  under UV excitation. It is also highly possible according to the Förster resonance ET (FRET) theory<sup>[17]</sup>, since the intense absorption band of  $\text{Eu}^{2+}$  and some emission lines of  $\text{Tb}^{3+}$  always overlap. Monitoring with 600-nm PL, one can observe a strong narrow excitation band peaked at 400-nm based on the broad excitation band. Such narrow and intense excitation band is assigned to the f-f transition of  $\text{Sm}^{3+}$ :  ${}^6\text{P}_{3/2} \rightarrow {}^6\text{H}_{5/2}$ , while the broad excitation band may also be due to ET from  $\text{Eu}^{2+}$  to  $\text{Sm}^{3+}$ . Thus, in the present system,  $\text{Eu}^{2+}$  ions and  $\text{Tb}^{3+}$  and  $\text{Sm}^{3+}$  ions act as donors and acceptors, respectively.

The PL intensities of the glass ceramics are enhanced to more than 5 times of those of the glass, as shown in Fig. 3. It is mainly derived from the enrichment of  $\text{Eu}^{2+}$ ,  $\text{Tb}^{3+}$  and  $\text{Sm}^{3+}$  into the precipitated  $\text{Ba}_2\text{LaF}_7$  phase. There are two processes that influence the PL of samples: one is the multiphonon relaxation (MPR), and the other is the ET. The MPR probability,  $W_{\text{MPR}}$ , depends primarily upon the energy gap between two successive levels ( $\Delta E$ ) and the maximum phonon energy of host ( $\hbar\omega$ )<sup>[18]</sup>. Excluding environment temperature, a relationship between  $W_{\text{MPR}}$  and the maximum phonon energy of host,  $\hbar\omega$ , exists and is given by<sup>[19]</sup>

$$W_{\text{MPR}} = W_0 \exp\left(-\frac{\alpha\Delta E}{\hbar\omega}\right), \quad (2)$$

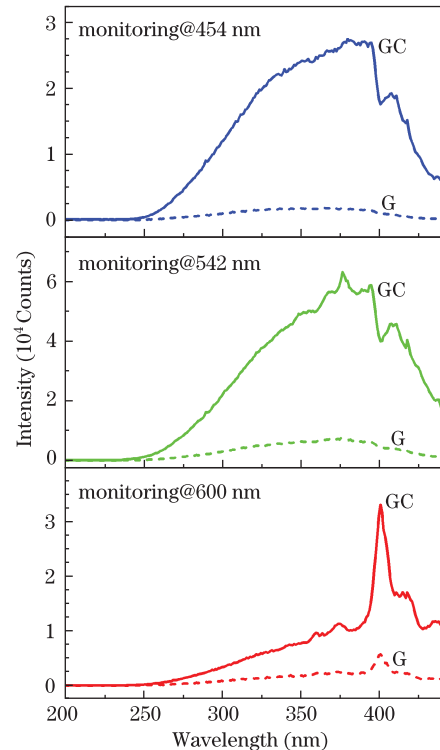


Fig. 3. Excitation spectra of the glass (G, short dash lines) and glass ceramics (GC, solid lines), by monitoring the  $\text{Eu}^{2+}$ ,  $\text{Tb}^{3+}$ , and  $\text{Sm}^{3+}$  luminescence at 454, 542, and 600 nm, respectively.

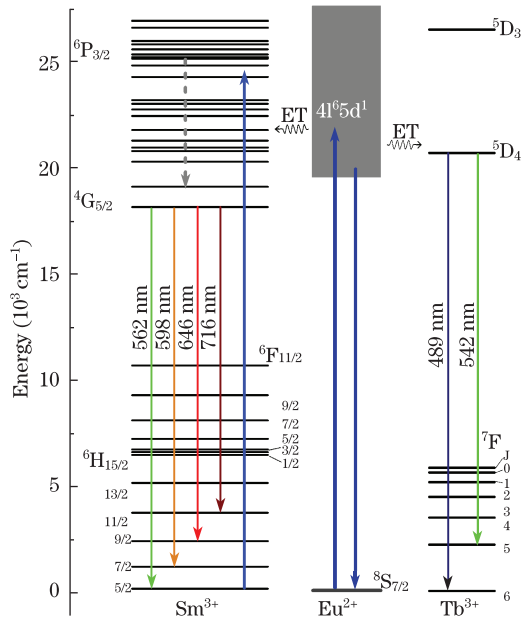


Fig. 4. Luminescence rising and decay curves of the glass (G, short dash lines) and glass ceramics (GC, solid lines), by monitoring 454-nm PL of  $\text{Eu}^{2+}$  with excitation from a 405-nm picosecond pulsed diode laser, and 576-nm PL of  $\text{Tb}^{3+}$  and 600-nm PL of  $\text{Sm}^{3+}$  with excitation from a 405-nm Xe flash lamp.

where  $W_0$  and  $\alpha$  are constants determined by the host type. Thus, the lower  $\hbar\omega$  leads to smaller  $W_{\text{MPR}}$ . Due to the much smaller  $\hbar\omega$  of  $\text{Ba}_2\text{LaF}_7$  nanocrystals ( $\sim 350 \text{ cm}^{-1}$ ) than silicate matrix ( $\sim 1100 \text{ cm}^{-1}$ ),  $W_{\text{MPR}}$  can be very low and the efficient emission can be expected for the glass ceramics. According to the energy transfer theory<sup>[17,20]</sup>, the ET probability has the following relationship with the distances between the donor and acceptor ions ( $r_{\text{D-A}}$ )

$$W_{\text{ET}} \propto 1/r_{\text{D-A}}^6. \quad (3)$$

The ET processes can be strengthened by the much closer inter-ionic distance brought about by the enrichment of  $\text{Eu}^{2+}$ ,  $\text{Tb}^{3+}$  and  $\text{Sm}^{3+}$  into the precipitated  $\text{Ba}_2\text{LaF}_7$  phase. As a result, the PL of acceptors ( $\text{Tb}^{3+}$  and  $\text{Sm}^{3+}$ ) is enhanced, while that of donors ( $\text{Eu}^{2+}$ ) is weakened. However, the emission assigned to  $\text{Eu}^{2+}$  of the glass ceramics is also stronger than that of glass, which is related to the increased number of stable  $\text{Eu}^{2+}$  ions existing in the glass ceramics owing to  $\text{Eu}^{2+}$  substituting  $\text{Ba}^{2+}$  sites in  $\text{Ba}_2\text{LaF}_7$ .

The abovementioned excitation and ET processes are illustrated as up and wave arrows in Fig. 4, respectively. In order to confirm these mechanisms, we also investigate the PL decay curves of samples, as shown in Fig. 5. The luminescence decays of  $\text{Tb}^{3+}$  yield a nearly single exponential decay, whereas the luminescence decays of  $\text{Eu}^{2+}$  and  $\text{Sm}^{3+}$  are non-exponential. Using the formula,  $\tau = \int t \cdot I(t) dt / \int I(t) dt$ , the average luminescence lifetime can be evaluated, where  $I(t)$  is the luminescence intensity at time  $t$ . The calculated lifetimes of  $\text{Eu}^{2+}$ ,  $\text{Tb}^{3+}$  and  $\text{Sm}^{3+}$  in the glass and glass ceramics are listed in Table 1. Based on the radiative rate theory<sup>[21]</sup>, the luminescence lifetime,  $\tau$ , has the following relationship with the probability of radiative transition ( $W_{\text{R}}$ ) and

non-radiative transitions (mainly including  $W_{\text{MPR}}$  and  $W_{\text{ET}}$ )

$$\frac{1}{\tau} = W_{\text{R}} + W_{\text{MPR}} + W_{\text{ET}} + \dots \quad (4)$$

For the glass ceramics, ET processes from  $\text{Eu}^{2+}$  to  $\text{Tb}^{3+}$  and  $\text{Sm}^{3+}$  depopulates the excited  $\text{Eu}^{2+}$  much more than the glass; thus, the  $\tau_{\text{Eu}^{2+}}$  of the glass ceramics (216.8  $\mu\text{s}$ ) is shorter than that of the glass (345.9  $\mu\text{s}$ ). On the contrary,  $\tau_{\text{Sm}^{3+}}$  of the glass ceramics (2.115 ms) is longer than that of the glass (1.521 ms), because the main factor for the PL of  $\text{Sm}^{3+}$  may be the weakened multiphonon relaxation in the glass ceramics. Moreover, the decay curves of  $\text{Tb}^{3+}$  in the glass and glass ceramics overlap so largely that we can hardly distinguish them. Thus, the lifetime difference of  $\text{Tb}^{3+}$  is slight, which is

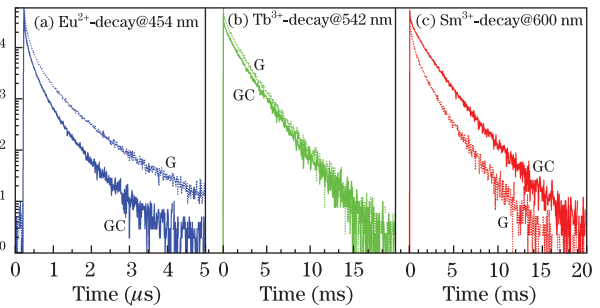


Fig. 5. Simplified energy level diagrams of  $\text{Eu}^{2+}$ ,  $\text{Tb}^{3+}$  and  $\text{Sm}^{3+}$ , and a possible ET mechanism from  $\text{Eu}^{2+}$  to  $\text{Tb}^{3+}$  and  $\text{Sm}^{3+}$ .

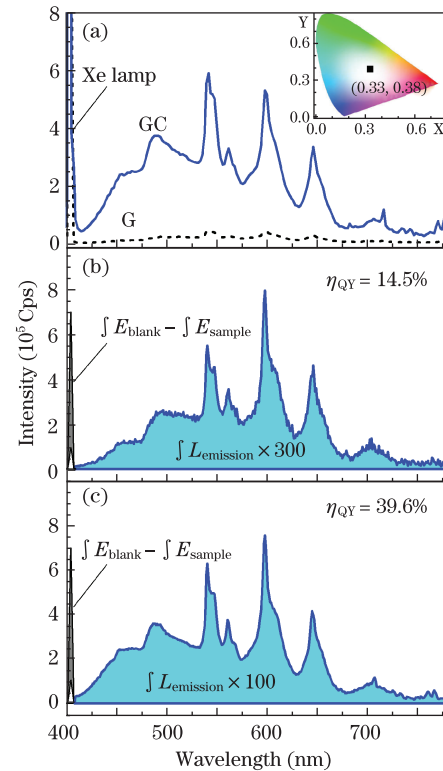


Fig. 6. Emission spectra of (a) the glass and glass ceramics, and emission spectra of (b) the glass and (c) glass ceramics recorded by an integrating sphere. Inset of (a) shows the CIE coordinates of the glass ceramics.

**Table 1 Lattice Parameters ( $a$ ) of Cubic  $\text{Ba}_2\text{LaF}_7$  Nanocrystals and the Luminescence Lifetimes of  $\text{Eu}^{2+}$  ( $\tau_{\text{Eu}^{2+}}$ ),  $\text{Tb}^{3+}$  ( $\tau_{\text{Tb}^{3+}}$ ), and  $\text{Sm}^{3+}$  ( $\tau_{\text{Sm}^{3+}}$ ) in the Samples**

Sample	$a$ (Å) <sup>a</sup>	$\tau_{\text{Eu}^{2+}}$ ( $\mu\text{s}$ ) <sup>b</sup>	$\tau_{\text{Tb}^{3+}}$ (ms) <sup>c</sup>	$\tau_{\text{Sm}^{3+}}$ (ms) <sup>d</sup>
Glass		345.9	2.064	1.521
Glass Ceramics	6.045	216.8	2.091	2.115

<sup>a</sup> Standard value is 6.088 Å (PDF# 48-0099).

<sup>b</sup> Monitoring 454 nm PL of  $\text{Eu}^{2+}$  with excitation from a 405 nm picosecond pulsed diode laser.

<sup>c</sup> Monitoring 576 nm PL of  $\text{Tb}^{3+}$  with excitation from a 405 nm Xe flash lamp.

<sup>d</sup> Monitoring 600 nm PL of  $\text{Sm}^{3+}$  with excitation from a 405 nm Xe flash lamp.

mainly because  $W_{\text{MPR}}$  of  $\text{Tb}^{3+}$  is not so sensitive to the phonon energy. This can also be deduced from the energy level positions of  $\text{Tb}^{3+}$  that are not as dense as  $\text{Sm}^{3+}$  at the range lower than 25 000  $\text{cm}^{-1}$ .

Figure 6(a) shows the emission spectra of the  $\text{Eu}^{2+}/\text{Tb}^{3+}/\text{Sm}^{3+}$  co-doped glass and glass ceramics. The broad emission band is assigned to the 5d→4f transition of  $\text{Eu}^{2+}$  ions, while the sharp emission peaks are assigned to the transitions of  $\text{Tb}^{3+}$ :  $^5\text{D}_4 \rightarrow ^7\text{F}_6$  (489 nm),  $\text{Tb}^{3+}$ :  $^5\text{D}_4 \rightarrow ^7\text{F}_5$  (542 nm),  $\text{Sm}^{3+}$ :  $^4\text{G}_{5/2} \rightarrow ^6\text{H}_{5/2}$  (562 nm),  $\text{Sm}^{3+}$ :  $^4\text{G}_{5/2} \rightarrow ^6\text{H}_{7/2}$  (598 nm), and  $\text{Sm}^{3+}$ :  $^4\text{G}_{5/2} \rightarrow ^6\text{H}_{9/2}$  (646 nm). Such emission is labelled using down arrows in Fig. 4. The emission intensity of the glass ceramics is much stronger than that of the glass due to the enrichment of rare earth ions into the precipitated  $\text{Ba}_2\text{LaF}_7$  nanophase. The inset graph of Fig. 6 (a) shows the Commission Internationale de l'Éclairage (CIE) chromaticity coordinates of the emission of the glass ceramics. According to the 1931 CIE-XYZ Coordinate System<sup>[22]</sup> of the CIE, the CIE coordinates of the emission of the glass ceramics, including the excitation source line, are calculated as (0.33, 0.38). Thus, it falls into warm white light region and is suitable for indoor high power illumination.

To study the real influence of crystallization on the PL, emission spectra were measured using an integrating sphere with a 405-nm Xe lamp excitation, as shown in Figs. 6(b) and (c). According to Eq. (1), the quantum yields (QYs) of the glass and glass ceramics are determined as 14.5% and 39.6%, respectively. In addition, the QY is improved largely after the annealing processes, due to the abovementioned microstructure and ionic distribution evolution. Therefore, we can demonstrate the presented glass ceramics as a potential candidate for WLED luminescent materials.

In conclusion, the  $\text{Eu}^{2+}$ ,  $\text{Tb}^{3+}$  and  $\text{Sm}^{3+}$  co-doped glass and glass ceramics containing cubic  $\text{Ba}_2\text{LaF}_7$  nanocrystals are prepared. By annealing processes,  $\text{Eu}^{2+}$ ,  $\text{Tb}^{3+}$  and  $\text{Sm}^{3+}$  ions are enriched into the precipitated  $\text{Ba}_2\text{LaF}_7$  nanophase. It deduces efficient ETs from  $\text{Eu}^{2+}$  to  $\text{Tb}^{3+}$  and  $\text{Sm}^{3+}$  in the glass ceramics. Thus, the glass ceramics emits a combination of red, green, and blue light under 405-nm excitation and exhibited white

light with CIE coordinates of (0.33, 0.38). The luminescence QY of the glass ceramics is also improved to a relatively large value of 39.6% due to the microstructure and ionic distribution evolution. Therefore, the presented glass ceramics can be considered as a potential candidate for WLED luminescent materials.

This work was supported by the National Nature Science Foundation of China (No. 50902120), the Research Fund of the Doctoral Program of Higher Education of China (No. 20100101120025), the Science and Technology Innovative Research Team of Zhejiang Province (No. 2009 R50010), and the Program for Changjiang Scholars and Innovative Research Team in the University.

## References

1. M. R. Krames, O. B. Shchekin, R. Mueller-Mach, G. O. Mueller, Z. Ling, G. Harbers, and M. G. Craford, *J. Disp. Technol.* **3**, 160 (2007).
2. T. Taguchi, *IEEE T. Electr. Electr.* **3**, 21 (2008).
3. S. Pimputkar, J. S. Speck, S. P. DenBaars, and S. Nakamura, *Nat. Photon.* **3**, 180 (2009).
4. S. Nakamura and B. Kramer, Present status of InGaN-based UV/blue/green LEDs and laser diodes *Advances, in Solid State Physics 38*, (Springer Berlin, Heidelberg, 1999) pp. 1-14.
5. J. K. Sheu, S. J. Chang, C. H. Kuo, Y. K. Su, L. W. Wu, Y. C. Lin, W. C. Lai, J. M. Tsai, G. C. Chi, and R. K. Wu, *IEEE Photon. Technol. Lett.* **15**, 18 (2003).
6. C.-K. Chang and T.-M. Chen, *Appl. Phys. Lett.* **91**, 081902 (2007).
7. G. J. Gao, N. Da, S. Reibstein, and L. Wondraczek, *Opt. Express* **18**, A575 (2010).
8. S. Fujita, A. Sakamoto, and S. Tanabe, *IEEE J. Sel. Top. Quantum Electron.* **14**, 1387 (2008).
9. D. Chen, Y. Yu, P. Huang, H. Lin, Z. Shan, and Y. Wang, *Acta Mater.* **58**, 3035 (2010).
10. D. Chen, Y. Wang, K. Zheng, T. Guo, Y. Yu, and P. Huang, *Appl. Phys. Lett.* **91**, 251903 (2007).
11. H. Lin, D. Chen, Y. Yu, Z. Shan, P. Huang, Y. Wang, and J. Yuan, *J. Appl. Phys.* **107**, 103511 (2010).
12. D. Chen, Y. Yu, H. Lin, P. Huang, F. Weng, Z. Shan, and Y. Wang, *Opt. Lett.* **34**, 2882 (2009).
13. Y. Wang and J. Ohwaki, *Appl. Phys. Lett.* **63**, 3268 (1993).
14. P. A. Tick, *Opt. Lett.* **23**, 1904 (1998).
15. Y. Q. Li, A. C. A. Delsing, G. De With, and H. T. Hintzen, *Chem. Mater.* **17**, 3242 (2005).
16. P. Dorenbos, *J. Lumin.* **104**, 239 (2003).
17. T. Forster, *Naturwissenschaften* **33**, 166 (1946).
18. S. Tanabe, K. Tamai, K. Hirao, and N. Soga, *Phys. Rev. B* **47**, 2507 (1993).
19. T. Miyakawa and D. L. Dexter, *Phys. Rev. B* **1**, 2691 (1970).
20. D. L. Dexter, *J. Chem. Phys.* **21**, 836 (1953).
21. S. Tanabe, S. Yoshii, K. Hirao, and N. Soga, *Phys. Rev. B* **45**, 4620 (1992).
22. M. Shaw and M. Fairchild, *Color. Res. Appl.* **27**, 316 (2002).